MULTIMODE DIFFRACTION TOMOGRAPHY WITH ELASTIC WAVES

Th. Kreutter and K.J. Langenberg

Dept. Electrical Engineering
University of Kassel
Wilhelmshöherallee 71
D-3500 Kassel, FRG

INTRODUCTION

In recent years ultrasonic imaging procedures have been developed to quantify defects [1,2,3,4] for application in QNDE or medical imaging. The demands for these purposes are high resolution images, true recovering of the scattering geometry and fast computer processing. But most of the published algorithms require certain assumptions as: plane wave excitation, measurements in the farfield of the scatterer or, which is a very serious restriction, scalar wave propagation.
To overcome these problems we have developed a more general framework of elastodynamic inverse scattering theory, which incorporates mode conversion and full elastic wave propagation phenomena[5]. Additionally most of the necessary processing steps can be done by utilizing mainly Fourier transforms. Therefore the algorithms are well suited for computer implementation in the cases of plane or cylindrical apertures.

BASIC EQUATIONS OF ELASTODYNAMICS

The wave equation for the displacement vector $\mathbf{u}$ reads [6]

$$(\lambda + \mu)\nabla\nabla \cdot \mathbf{u} + \mu\Delta\mathbf{u} + \rho\omega^2\mathbf{u} = -\mathbf{f} \tag{1}$$

where λ, μ are the Lamé's constants, ρ is the mass density, $\mathbf{f}$ accounts for the volume force density and ω denotes the circular frequency if we assume a time dependance $\sim e^{-j\omega t}$. Additionally, we have an equation for the Green's displacement tensor [6] - $\mathbf{I}$ being the identity dyadic operator

$$(\lambda + \mu)\nabla\nabla \cdot \mathbf{G} + \mu\Delta\mathbf{G} + \rho\omega^2\mathbf{G} = -\delta\mathbf{I} \tag{2}$$

and for a third rank Green's tensor

$$\nabla \cdot \mathbf{\Sigma} + \rho\omega^2\mathbf{G} = -\delta\mathbf{I} \tag{3}$$

If we introduce a Helmholtz decomposition of $\mathbf{u}$

$$\mathbf{u} = \nabla\Phi + \nabla \times \mathbf{\Psi} \text{ ; with } \nabla \cdot \mathbf{\Psi} = \mathbf{0} \tag{4}$$

and $\mathbf{f}$

$$\mathbf{f} = (\lambda + 2\mu)\nabla f_\Phi + \mu\nabla \times \mathbf{f}_\Psi \text{ ; with } \nabla \cdot \mathbf{f}_{\mathbf{\Psi}} = 0 \tag{5}$$

we get two differential equations for the potential Φ and the vector potential $\mathbf{\Psi}$

$$(\Delta + k_P^2)\phi = -f_\Phi \tag{6}$$

Review of Progress in Quantitative Nondestructive Evaluation, Vol. 9
Edited by D.O. Thompson and D.E. Chimenti
Plenum Press, New York, 1990

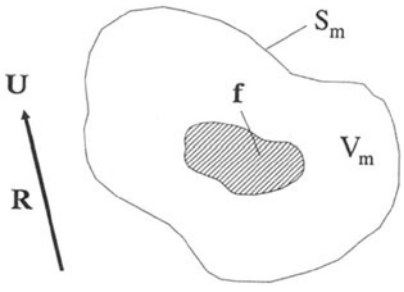

Figure 1. Geometry for the Huygens' principle

$$(\Delta + k_S^2)\Psi = -\mathbf{f}_\Psi \tag{7}$$

where $k_P = \omega^2\rho/(\lambda + 2\mu)$ denotes the wavenumber of the Pressure- and $k_S = \omega^2\rho/\mu$ is the wavenumber of the Shear-wave. Hence all quantities in eq.(1-3) can be decomposed into a pressure and shear wave distribution

$$\mathbf{u} = \mathbf{u}^P + \mathbf{u}^S, \mathbf{G} = \mathbf{G}^P + \mathbf{G}^S, \text{ and } \boldsymbol{\Sigma} = \boldsymbol{\Sigma}^P + \boldsymbol{\Sigma}^S \tag{8}$$

Alternatively, we are able to formulate an integral equation relating to Huygens' principle [6]

$$-\int_{S_m} (\mathbf{nu} : \boldsymbol{\Sigma} - \mathbf{n} \cdot \mathbf{T} \cdot \mathbf{G})\, dS_m + \int_{V_m} \mathbf{f} \cdot \mathbf{G}\, dV_m = \begin{cases} \mathbf{u} & ;\mathbf{R} \in V_m \\ \frac{\mathbf{u}}{2} & ;\mathbf{R} \in S_m \\ \mathbf{0} & ;\mathbf{R} \notin V_m \end{cases} \tag{9}$$

where V_m and S_m are illustrated in Fig. 1, $\mathbf{n}$ denotes the outer normal of S_m, and $\mathbf{T}$ being the stress tensor. According to eq.(8) we can specialize eq.(9) to

$$\mathbf{u}_s^\beta = \int_{S_m} (\mathbf{nu} : \boldsymbol{\Sigma}^\beta - \mathbf{n} \cdot \mathbf{T} \cdot \mathbf{G}^\beta)\, dS_m \; ; \; \mathbf{R} \notin V_m \; ; \; \beta = \text{ P, S} \tag{10}$$

Therefore, by integrating over some known field distribution on the surface S_m and using only the Green's function of a certain wave mode we yield exactly the displacement which belongs to this wave mode. Thus, it is possible to perform a wave mode separation, which will be important in the next chapter.

ELASTODYNAMIC INVERSE SCATTERING, PROBLEMS AND ITS SOLUTIONS

Consider a scatterer with a stress free boundary condition on its surface S_c

$$\mathbf{n} \cdot \mathbf{T} = \mathbf{t} = 0 \text{ on } S_c \tag{11}$$

as shown in Fig. 2, which is illuminated by a source moving on the surface S_i generating the incident displacement $\mathbf{u}_i$; on the surface S_m we have a receiver to measure the scattered wave field $\mathbf{u}_s$. If we apply an eq. similar to eq.(9) to the surface of the scatterer S_c inserting the appropriate boundary condition and changing the surface integral with the definition of the singular function: $\gamma = -\mathbf{n} \cdot \nabla\Gamma$ to a volume integral with respect to V_c , the volume of the scatterer, we get

$$\mathbf{u}_s = \int_{S_m} (\mathbf{nu} : \boldsymbol{\Sigma} - \mathbf{n} \cdot \mathbf{T} \cdot \mathbf{G}) dS_m = \int_{S_c} \mathbf{nu} : \boldsymbol{\Sigma} dS_c = \int_{V_c} \gamma \mathbf{nu} : \boldsymbol{\Sigma} dV_c \tag{12}$$

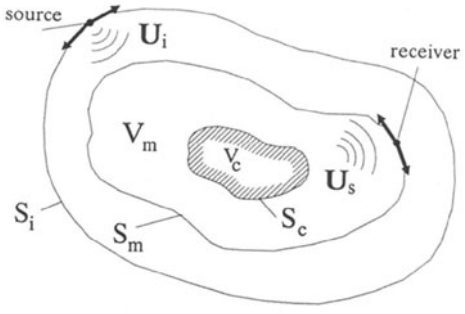

Figure 2. Geometry for the inverse problem

with

$$\gamma(\mathbf{R}) = -\mathbf{n} \cdot \nabla\Gamma(\mathbf{R});\ \Gamma(\mathbf{R}) = \begin{cases} 1 & ;\ \mathbf{R} \text{ inside the scatterer} \\ 0 & ;\ \mathbf{R} \text{ outside the scatterer} \end{cases} \tag{13}$$

Eq.(12) formulates the inverse problem we have to solve:
On the left hand side, the scattererd wave field $\mathbf{u}_s$ is given in terms of measurable quantities on the surface S_m, which is related on the right hand side via a volume integral to the singular function exhibiting the geometry of the scatterer.
To invert eq.(12) we would like to transform it into a Fourier integral; but to do this, some problems have to be overcome. The integral equation

$$\mathbf{u}_s = \int_{V_c} \gamma \mathbf{n}\mathbf{u} : \mathbf{\Sigma} dV_c \tag{14}$$

is not linear with regard to γ because $\mathbf{u}\,|_{Sc}$ is also unknown and depends on γ. Here, we apply the method of physical elastodynamics [5] to approximate the surface displacement in terms of $\mathbf{u}_i$ which is given. Doing measurements we generally get mixed wave modes $\mathbf{u} = \mathbf{u}_P + \mathbf{u}_S$ with different propagation characteristics. As mentioned in the previous chapter, eq.(10) decomposes the measured displacement vector $\mathbf{u}$. It is important to notice, that in the case of plane or cylindrical apertures (which are often used in practical experiments, for instance turbine shafts) the integration over S_m can be performed very efficiently using Fourier transforms of the measured displacement; also the surface stress can be expressed in terms of $\mathbf{u}$, so that we need only measurements of the displacement itself for this special application.
If the location of the sources or the receivers is in the nearfield we have no Fourier kernel in eq.(14), hence we design filter operations [1] to simulate measurement and excitation in the farfield, so that we can deal computionally with plane waves. In the case of cylindrical or plane apertures these operations are also performed utilizing Fourier transforms.
Finally we obtain

$$\mathbf{u}_{\alpha\beta}^{comp}(\omega, \hat{\mathbf{R}}, \hat{\mathbf{R}}_i) = \int_{V_c} \mathbf{C}_{\alpha\beta} \gamma e^{j(-k_\alpha \hat{\mathbf{R}}_i + k_\beta \hat{\mathbf{R}}) \cdot \mathbf{R}'} dV_c' \tag{15}$$

where $\mathbf{u}_{\alpha\beta}^{comp}$ denotes the displacement as computed from measurements due to the processing steps. $\mathbf{C}_{\alpha\beta}$ is the vectorial result of the dyadic product of $\mathbf{nu} : \mathbf{\Sigma}$ in terms of the method of physical elastodynamics, whence the exponential phase term. α, β = P, S are the modes of the incident and measured wave, respectively. $\hat{\mathbf{R}}$, $\hat{\mathbf{R}}_i$ denote the unit vectors into observation and excitation direction.
To get the vector $\mathbf{C}_{\alpha\beta}$ out of the integral we apply the method of stationary phase [7] and yield

$$\mathbf{u}_{\alpha\beta}^{comp}(\omega, \hat{\mathbf{R}}, \hat{\mathbf{R}}_i) = \mathbf{C}_{\alpha\beta}(\hat{\mathbf{R}}, \hat{\mathbf{R}}_i) \int_{V_c} \gamma e^{j(-k_\alpha \hat{\mathbf{R}}_i + k_\beta \hat{\mathbf{R}}) \cdot \mathbf{R}'} dV_c' \tag{16}$$

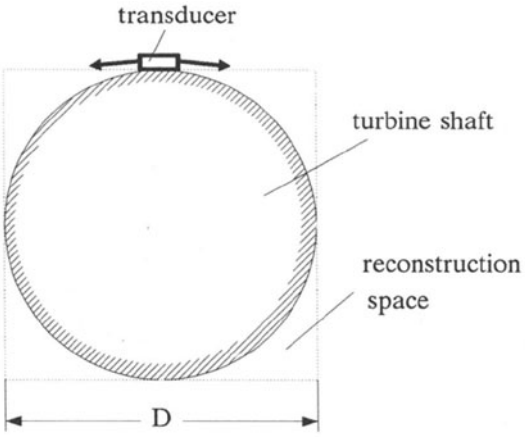

Figure 3. Monostatic multifrequency experiment $f_0 = 4.3\text{MHz}$, $c_P = 5920\frac{m}{s}$, $D = 369mm$, P-P mode

Finally we normalize the amplitude

$$\mathbf{u}_{\alpha\beta}^{comp} \cdot \frac{\mathbf{C}_{\alpha\beta}}{\mid \mathbf{C}_{\alpha\beta} \mid^2} = \tilde{\gamma}(\mathbf{K}) \tag{17}$$

and discover $\tilde{\gamma}(\mathbf{K})$ to be the threedimensional Fourier transform of $\gamma(\mathbf{R})$ defining a Fourier vector $\mathbf{K}$ through

$$\mathbf{K} = -k_\alpha \hat{\mathbf{R}}_i + k_\beta \hat{\mathbf{R}} \tag{18}$$

which is the instruction to fill K-space. So we end up with the elastodynamic inverse scattering algorithm

$$\gamma(\mathbf{R}) = \int_K \frac{\mathbf{u}_{\alpha\beta}^{comp} \cdot \mathbf{C}_{\alpha\beta}}{\mid \mathbf{C}_{\alpha\beta} \mid^2} e^{-j\mathbf{K}\cdot\mathbf{R}} dK \tag{19}$$

where the integral can be computed by multidimensional FFT.
At last we consider some special experimental configurations. If a fixed farfield source is used (plane wave) we have to sweep the frequency according to eq.(18) to fill K-space. In the case of a fixed nearfield source (point or line source) we have to vary the frequency and to apply an additional inverse Radon transform [2]. If we deal with monostatic or impulse echo experiments, which is the most popular practical configuration, we measure transient impulses and apply a Fourier transform with respect to time to fill K-space. This is the elastodynamic Fourier transform version of the classical scalar time domain SAFT, and which has been termed FT-SAFT [8]

EXPERIMENTAL AND NUMERICAL RESULTS

The first result is an example for a practical QNDT problem, the imaging of the cross-section of a turbine shaft, as shown in Fig. 3. This is a monostatic multifrequently experiment,

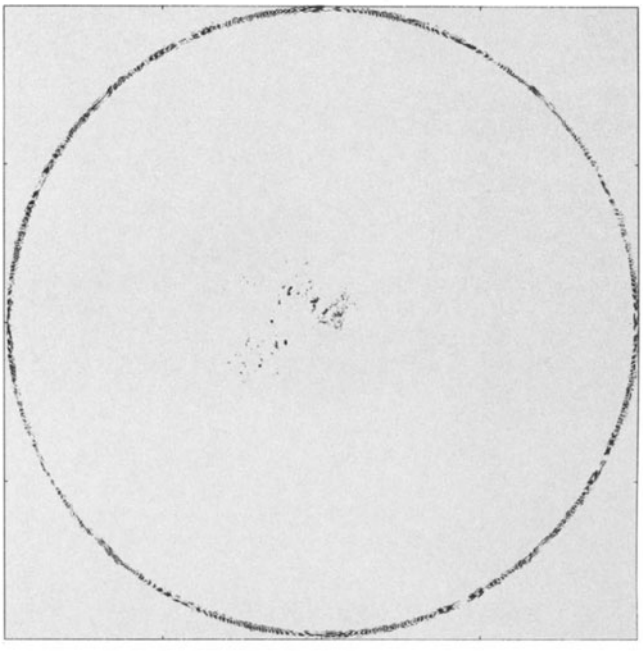

Figure 4. Image of the turbine shaft cross-section

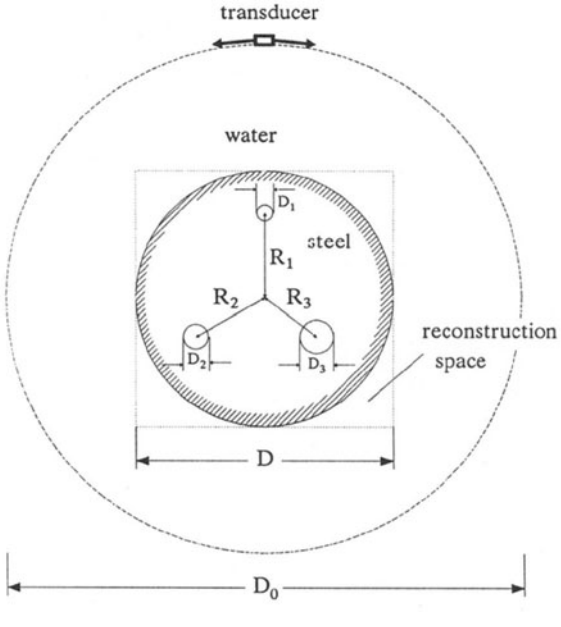

Figure 5. Monostatic multifrequency experiment $f_0 = 2.25$ MHz , $c_{P,water} = 1480\frac{m}{s}$, $c_{P,steel} = 5690\frac{m}{s}$, $D = 80mm$, $D_0 = 148mm$ $D1 = 2mm$, $D2 = 4mm$, $D3 = 6mm$, $R1 = 30mm$, $R2 = 25mm$, $R3 = 20mm$, P-P mode

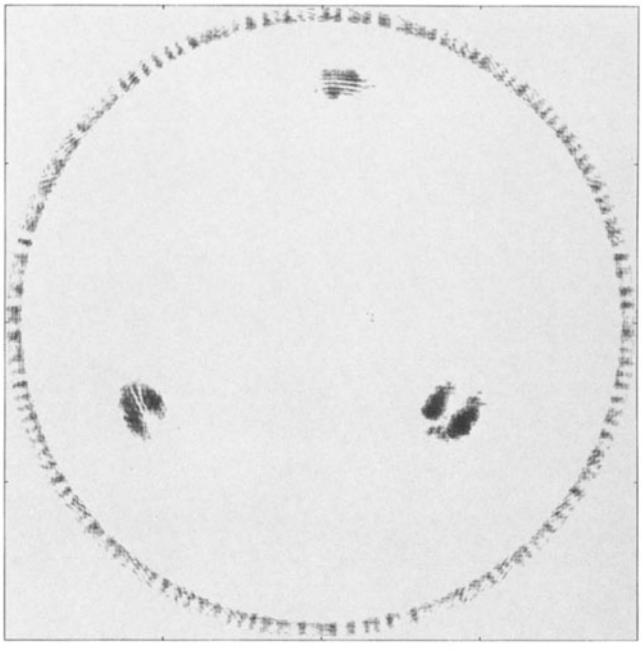

Figure 6. Cross-section Image

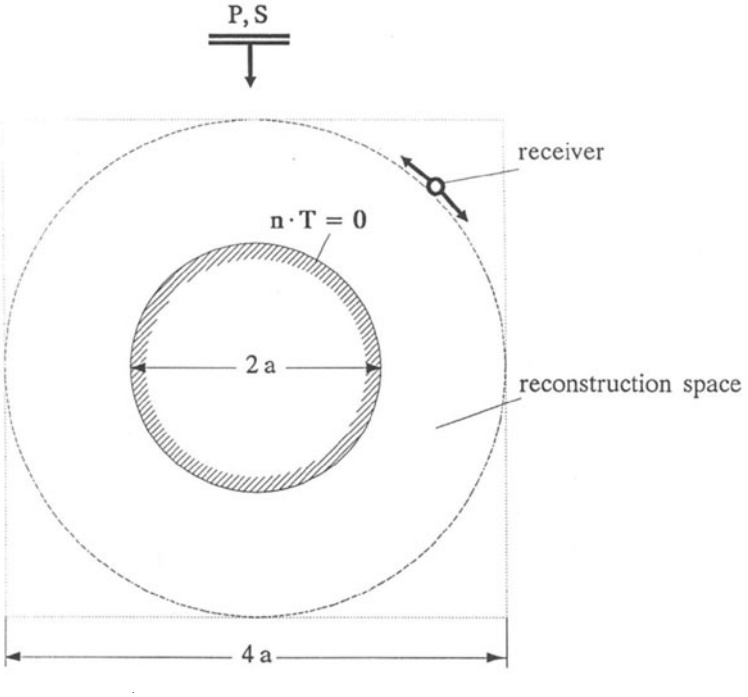

Figure 7. Bistatic multifrequency experiment $0 \leq k_P a \leq 40.$, $k_P = \frac{\omega}{c_P}$, $c_P = 5900\frac{m}{s}$, $c_S = 3200\frac{m}{s}$

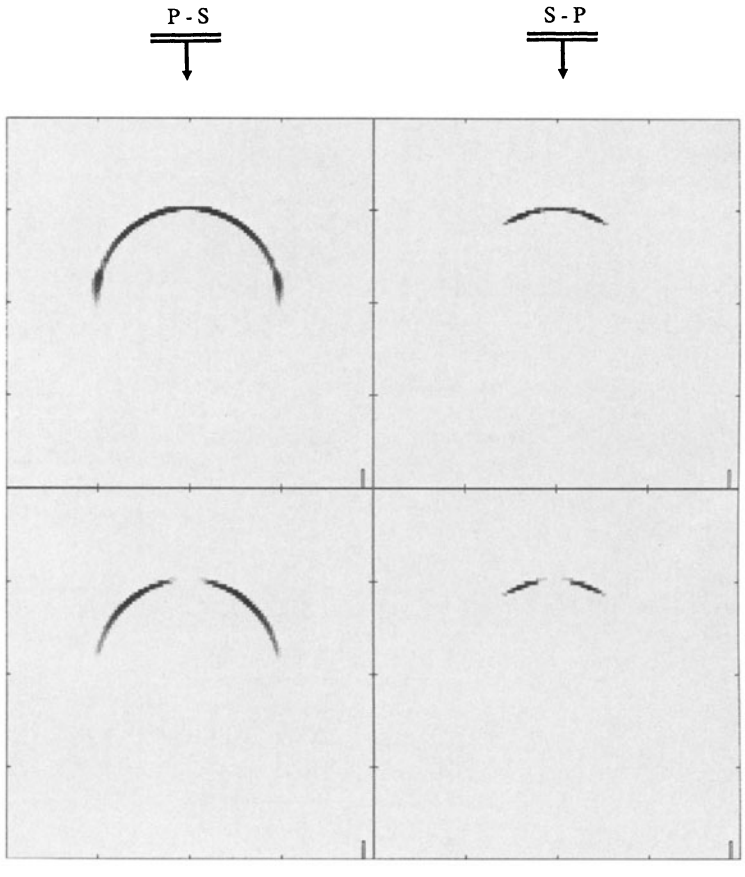

Figure 8. Bistatic multifrequency imaging

because we use one transducer and take the time domain data circumferentially. The result in Fig. 4 is shown in a grey scaled coding, we recognize the measurement surface and some natural small defect distribution in the center of the turbine shaft. The processing time is approximately a hundred times faster than conventional time domain SAFT-imaging.
The next example is based on the same technique, but the turbine shaft is embedded in water and inside the specimen there are three circular cylindrical drillings with different diameters and distances to the center, as illustratd in Fig. 5. Here, the measured displacement is first backpropagated to the surface of the turbine shaft with the speed of ultrasound in water and then we initialize the FT-SAFT algorithm. Fig. 6 shows the result, the limited resolution of the defects is due to the bandlimitation of the tranducer in space and frequency.
The last example is a computer simulation, where an analytical solution in terms of an eigenfunction expansion is used to calculate the scattered field of a cylinder with stress free boundary condition as shown in Fig. 7. We consider a fixed plane wave excitation and take multifrequency 'measurements' on a circular aperture. Fig. 8 shows on the left hand side the result for an incident plane wave with α = P and β = S, on the right hand side we have chosen α = S and β = P. The upper results hold for reconstruction via eq.(19) with amplitude normalisation and the lower results are referring to eq.(15) to show the effect of a quasi 'scalar' reconstruction.
The results illustrate, that only the illuminated and 'visible' region of the scatterer in the sense

of physical elastodynamics is imaged. Processing without amplitude normalisation yields a distribution which is closely related to the surface displacement on the cylinder [9]. Utilizing eq.(19) gives the 'complete' image of the illuminated geometry.

References

1 A.J. Devaney, G. Beylkin: Diffraction tomography using arbitrary transmitter and receiver surfaces. Ultrasonic Imaging **6** (1984) 181

2 C. Esmersoy, M.L. Oristaglio, B.C. Levy: Multidimensional Born velocity inversion: Single wideband point source. J. Acoust. Soc. Amer. **78** (1985) 1052-1057

3 G.T. Herman, H.K. Tuy, K.J. Langenberg, P. Sabatier: Basic Methods of Tomography and Inverse Problems. Adam Hilger, Techno House, Bristol (1987)

4 K. J. Langenberg: Introduction to the Special Issue on Inverse Problems. Wave Motion **11** (1989) 99-112

5 Th. Kreutter: Elastodynamische Inverse Beugungstheorie. Ph. D. Thesis, University of Kassel 1989 (in preparation)

6 Yih-Hsing Pao, V. Varatharajulu: Huygens' principle, radiation conditions, and integral formulas for the scattering of elastic waves. J. Acoust. Soc. Am., Vol. 59, No. 6 (1976) 1361-1371

7 N. Bleistein: Mathematical Methods for wave phenomena. Academic press, London (1984)

8 K.-Mayer, R. Marklein, K. J. Langenberg, T. Kreutter: A 3D ultrasonic imaging system based on FT-SAFT. Ultrasonics (1989) (to appear)

9 K.J. Langenberg, U. Aulenbacher, G. Bollig, P. Fellinger, H. Morbitzer, G. Weinfurter, P. Zanger, V. Schmitz: Numerical Modelling of Ultrasonic Scattering. In: Mathematical Modelling in Nondestructive Testing, Eds.: M. Blakemore, G.A. Georgiou, Clarendon Press, Oxford (1988)